The Faster the Better? Optimal Warm-Up Strategies for a Micro Combined Heat and Power Plant

energies

MDPI

Article

The Faster the Better? Optimal Warm-Up Strategies for a Micro Combined Heat and Power Plant

Tammo Zobel *, Andreas Ritter and Christopher H. Onder

Institute for Dynamic Systems and Control, ETH Zurich, Sonneggstrasse 3, 8092 Zurich, Switzerland; anritter@idsc.mavt.ethz.ch (A.R.)

* Correspondence: tzobel@idsc.mavt.ethz.ch

Abstract: The warm-up process is a critical operation phase for micro Combined Heat and Power (mCHP) plants, directly impacting their efficiency, reliability, and lifetime. As small decentralized power generation units are increasingly expected to be operated on demand, start-ups will occur more frequently and thus the importance of the warm-up process will further increase. In this study, we address this problem by presenting a mathematical optimization framework that finds optimal actuator trajectories that significantly reduce the warm-up time and improve the thermal efficiency of an mCHP plant. The proposed optimization framework is highly flexible and adaptable to various objective functions, such as maximizing efficiency or minimizing the deviation from desired temperature references. The underlying mathematical model has been experimentally validated on a physical mCHP test rig. Selected case studies further demonstrate the effectiveness and flexibility of the framework and show that with the optimized actuator trajectories, the mCHP plant can reach its steady-state operating temperature in 40% less time. The results also indicate that the shortest warm-up time does not necessarily lead to the highest thermal efficiency. Accordingly, the methodology proposed in this paper provides a powerful tool to study higher-level operational strategies of mCHP plants and thus to maximize their overall performance, which directly translates into an improved operational cost-effectiveness, particularly in demand-driven energy landscapes.

Keywords: combined heat and power; optimal control; hydraulic warm-up; cogeneration

Citation: Zobel, T.; Ritter, A.; Onder, C.H. The Faster the Better? Optimal Warm-Up Strategies for a Micro Combined Heat and Power Plant. *Energies* **2023**, *16*, 4180. https://doi.org/10.3390/en16104180

Academic Editor: Massimo Dentice D'Accadia

Received: 15 April 2023
Revised: 6 May 2023
Accepted: 11 May 2023
Published: 18 May 2023

1. Introduction

1.1. Motivation

The global energy transition challenges many countries to actively transform their energy landscapes into using minimal shares of fossil fuels [1]. Since regional and even sectoral conditions can vary widely, future energy solutions must adapt to these local requirements. Combined Heat and Power (CHP) plants can play a vital role in addressing this, as they are a decentralized form of energy generation units that provide both heat and electrical power close to the actual consumer [2,3]. CHP plants can also help ensure energy security because of their small transport losses, grid stabilization capabilities, and large variety of prime movers and thus fuels [4]. This allows the most locally appropriate CHP plants to be installed based upon on the available fuel variant [5,6]. The authors of [7] provide a comprehensive review on the technological capabilities within the CHP sector. One of the main upsides of CHP plants is their high total efficiency, ranging from around 80% to greater than 100%, if condensing technology is employed. The total efficiency is the sum of the thermal and electrical efficiency. While CHP plants generate electrical energy within seconds, the nominal thermal energy, and thus the maximum total efficiency, is only reached under steady-state conditions, i.e., when the CHP plant is fully warmed up. Until steady-state conditions are reached, a CHP plant only generates electrical energy, thus providing a total efficiency in the range of only 22% to 35%. Depending on the individual system the warm-up time often takes about 15 to 25 min, which means that CHP plants

spend a considerable amount of time operating at very low efficiencies. This effect naturally decreases with increasing runtime because of fewer start-up procedures and thus fewer warm-up conditions. However, the shift to more decentralization also means a shift to a more demand-driven operation, i.e., providing heat and power when required with minimal resources. This applies in particular to environments with fluctuating energy demand such as residential areas [8], where smaller units, i.e., so-called micro Combined Heat and Power (mCHP) plants, are suitable. The authors of [9] investigated the dynamic performance of CHP plants in the residential sector and conclude that their application can lead to substantial primary energy savings. However, this sector faces several challenges and needs that are comprehensively presented in [10]. Further adoption of mCHP plants in the residential sector currently faces numerous hurdles, including payback time, household energy demand, maintenance, sizing and capacity issues, and regulatory and safety issues. Accordingly, it is important to reduce the negative effects of low efficiency during the warm-up phase, as these effects have a significant impact on payback time, the ability to meet consumer energy demand in a timely fashion, and on maintenance. We believe that the application of mathematical optimization is ideally suited to tackling this issue in a systematic way. It allows for not only identifying optimal actuator trajectories that either maximize thermal efficiency or minimize warm-up times, but also to study the trade-offs between these two somewhat conflicting objectives. Furthermore, an optimization routine allows for deriving various online controllers, from simple Proportional Integral (PI) controllers that realize predefined actuator trajectories to more advanced control approaches, such as Model Predictive Control (MPC) [11,12]. MPC repeatedly solves the optimization problem on a receding horizon based on current measurement values to predict the future behavior of the plant and, thus, to arrive at a nearly optimal control strategy.

1.2. Prior Research

The warm-up or start-up phase has been the subject of prior research, particularly in applications that use a gas turbine as the prime mover. The authors of [13] focused directly on the start-up operation of the gas turbine, whereas [14] studied the cold-start behavior in the context of an Heat Recovery Steam Generator (HRSG) application. The authors of [15] were one of the first to utilize nonlinear MPC, and thus optimization methods, in CHP applications, followed by [16], which focused specifically on the start-up phase. The authors of [17] studied the modeling of combined cycle power plants for optimization purposes in more detail, whereas [18,19] extended prior work to set up entire optimization frameworks to study start-up applications. More recent research on optimization-based control of CHPs has focused on questions related to operational control, flexible loads, energy management, and specific use cases. The authors of [20] developed an economically optimal operation for real-time scheduling of CHP systems with energy storage. The authors of [21] reviewed technologies and optimal operation strategies through the lens of technical flexibility, whereas [22] focused on dynamic modeling and flexible load control for CHP units. The authors of [23] shed light on the modeling and optimization of CHP-related power dispatch challenges, whereas [24] extensively reviewed potential technologies to optimize the flexibility of CHP plants on a systemic level. The authors of [25] reviewed optimization approaches specifically in the sector of Combined Cooling, Heat and Power (CCHP) microgrids, while [26] examined optimal energy management by designing an operating cost minimization problem for microgrids with CHP generation, energy storage, and renewable energy resources. The authors of [27] applied the use of optimization methods in a specific real-world context by focusing on hospital structures. The authors of [28] applied mathematical optimization in the field of bottoming-cycle cogeneration, with the aim of achieving economic gains. The authors of [29] shed light on the application of optimization in multi-actor energy networks, and, in particular, compared centralized and decentralized energy generation units in multi-user buildings with electric and diesel vehicles. The authors of [30] studied multi-system energy generation

environments and exploited novel machine learning algorithms to optimize a power and freshwater cogeneration system.

1.3. Contributions of This Work

Cold-starts and subsequent warm-up processes are very common in many technical applications, particularly in energy generation units such as CHP plants. Existing approaches to accelerate the start-up process through the use of optimization-based methods focus on the prime mover, e.g., gas turbines, and do not target the transient hydraulic warm-up process that generates the hot water supply for heating applications. However, this warm-up phase is the main cause of low plant efficiency and will be crucially important for the economic viability of any energy generation unit in the course of increasingly demand-driven operation. In this study, we address this issue by evaluating the potential of minimizing the time it takes to reach the steady-state condition through an interplay of technical solutions and the application of mathematical optimization. Specifically, we develop an optimization framework based on a mathematical model of the physical mCHP test rig, which consists of a small set of parameters. We then showcase the framework's flexibility in a case study, where we utilize it to determine optimal control trajectories for the actuators, given various objectives and time constraints. Based on our results obtained, we study the potential benefits of accelerating the warm-up process and improving the overall thermal efficiency. We also quantify this potential by comparing the optimization results to a reference warm-up scenario that represents a very common hydraulic and operation setup for CHP plants. Our findings highlight the importance of mathematical optimization in improving the performance of CHP plants, provide insights for future research in this area, and generate practical implications for other types of hydraulic applications.

1.4. Methodology and Outline

Section 2 illustrates the experimental setup and highlights technological requirements and preconditions. Section 3 contains the mathematical description of the model employed in the optimization framework. The formulation of the optimization problem is explained in Section 4. The optimization framework is then applied in Section 5, using appropriate case studies, followed by an in-depth discussion of the results in Section 6. Section 7 sheds light on the practical implications of our study and discusses future advancements.

2. System Description

The experimental system is a prototype specifically developed to conduct research that addresses current drawbacks of mCHP plants. In the following, we describe the system by introducing its components, function principles, operation modes and limits.

2.1. System Components

Figure 1 illustrates the schematic structure of the micro Combined Heat and Power (mCHP) plant used in this study. The heart of the system is a single cylinder Internal Combustion Engine (ICE) with a displacement volume of 0.325 L. It runs on natural gas taken directly from the conventional natural gas grid. The amount of gas is controlled by means of an air/fuel ratio controller acting on the gas valve to provide stoichiometric conditions upstream of the Three-way Catalytic Converter (TWC). This mCHP plant is operated under full load at all times; thus, there is no throttle valve integrated into the air path. The engine shaft is coupled with a flywheel that smooths out the power delivery to an asynchronous generator. The generator converts the rotational kinetic energy to electrical energy. The hydraulic setup consists of two main circuits: the engine's cooling circuit and the water circuit. The cooling circuit, further denoted by subscript c, prevents the engine and the engine oil from overheating. The cooling fluid is regular water mixed with 25% ethylene glycol. The water circuit, further denoted by subscript w, provides a supply of hot water to the heating demand-side, in Figure 1 represented by a Thermal Energy Storage (TES), from which it is further distributed to individual appliances, e.g., space heaters or

hot water applications. Note that the TES is used as an illustrative example and the dashed line in Figure 1 represents the actual system boundary of the research conducted in this study. A secondary path provides a small water flow to cool the generator. Each circuit has an integrated centrifugal pump for fluid circulation. The central element connecting them is a plate heat exchanger (HXP). Within the HXP, heat is removed from the cooling circuit and transferred to the water circuit. A shell-and-tube heat exchanger with condensing technology, further referred to as heat exchanger exhaust gas (HXE), utilizes the energy of the hot exhaust gas by transferring heat energy to the heating water.

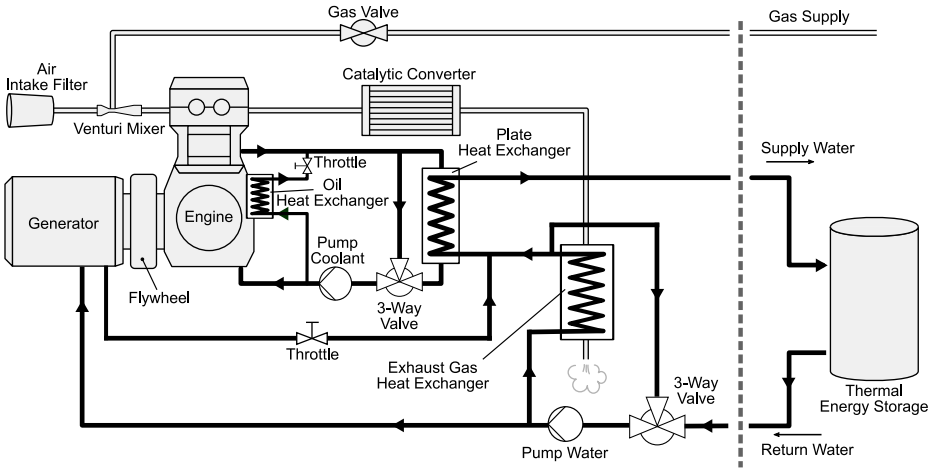

Figure 1. Schematic layout of the mCHP plant.

2.2. Sensors and Actuators

Up to this point, the hydraulic design is similar to many commercial CHP plants. The differentiating factor is the integration of two three-way valves, one in each hydraulic circuit. These ball valves can be continuously adjusted by the associated rotary actuators, thus enabling the cooling fluid and the heating water to partially or entirely bypass the HXP. In line with the scope of this study, i.e., to minimize the time it takes to reach steady-state conditions, each of the valves introduces an additional degree of freedom to control the heat flow from the cooling circuit to the water circuit. The two valves are complemented by the two centrifugal pumps, meaning that the hydraulic system incorporates four actuators. The sensoric equipment for this research includes various thermocouple sensors and flow meters. All sensor signals are available on the Controller Area Network (CAN) bus. The Electronic Control Unit (ECU) interfaces to all actuators and the test rig computer, pools all sensoric data, and runs all low-level controllers to ensure a safe, reliable, and stable operation. Table A1 provides more detailed information on the test rig hardware.

2.3. Operation

As soon as the mCHP receives a start signal, the asynchronous generator connects to the electricity grid. By design, the generator attempts synchronization, and as a result drags the engine close to the operating speed. After less than 10 s synchronization is complete and the ignition is switched on. From this point on, the engine delivers mechanical power to the asynchronous generator, which generates the electrical energy. The thermal energy of the combustion process produces hot exhaust gases and warms up the engine. As already mentioned, this thermal energy is harnessed in both ways via one heat transfer each in the plate and shell-and-tube heat exchanger to warm up the heating water. In practice, the warm-up process is often determined by the system design. Further fine tuning is usually performed by experience and knowledge of the responsible control engineers and does not involve mathematical tools to ensure optimal system behavior.

3. Modeling Approach

3.1. Application

As highlighted in Section 1, the objective of this study is to minimize the time it takes from a cold-start to achieving steady-state conditions at which thermal energy can be supplied to the heating demand-side. In other words, we aim to apply mathematical optimization methods to find optimal actuator trajectories for the centrifugal pumps and the three-way valves that enable the CHP plant to reach a desired final temperature state in the shortest time possible. In this study, we define the steady-state condition, i.e., the desired final state, as the operating point at which the supply water temperature reaches the reference temperature ϑ_{ref}^{out}. We set $\vartheta_{ref}^{out} = 80\,°C$ for two reasons in this study. First, 80/60 and 80/30 are common supply/return temperature setups in buildings that have radiators as space heaters. Second, to effectively compare the achieved results we need a fixed set of boundary conditions. We thus use the system boundary in Figure 1 (dashed line) as a reference frame and fix the return temperature to $\vartheta_{chp}^{in} = 30\,°C$ and the temperature of the surrounding air to $\vartheta_{air} = 30\,°C$. This measure eliminates any external influences on the warm-up dynamics, thereby facilitating the quantitative evaluation of the results.

3.2. Assumptions

Many studies have developed models of CHP plants for either general, e.g., [31,32], or specific control purposes [15,17,19,25,27]. Our modeling approach aims to identify and focus on the key elements that lead to a potential increase in energy efficiency. We therefore aim to use models with low complexity that maintain sufficient accuracy to capture the relevant thermal dynamics during the warm-up phase. This approach favors both an application in a mathematical optimization environment and significant reduction in system identification efforts. We made the following simplifications: First, we omit the electric power generation since our objective focuses on the thermal energy production. Second, we leave out the fluid paths through the generator and the oil heat exchanger (Figure 1). Both of these mass flows are less than 5% of their main circuit mass flows during the entire range of operation. Therefore, we neither model the generator, nor the oil heat exchanger, nor the flywheel. Third, the CHP plant is assumed to operate under close-to-stoichiometric conditions due to the TWC. The air/fuel ratio controller reaches operating conditions within a few seconds. Additionally, the CHP plant is operated at full load at all times. Thus, we ignore the impact of the initial transient air path dynamics on the thermal behavior of the hydraulic system and assume both constant air and constant fuel mass flows. Hence, we can model the heat transfer from the combustion chamber to the engine block as a constant parameter $\dot{Q}_{comb,e}$. In line with these assumptions, we also model the exhaust gas mass flow $\dot{m}_{exh}$ as a fixed constant parameter. In contrast to the CHP plant layout in Figure 1, this set of assumptions results in a model that consists of two main hydraulic circuits: (1) the engine's coolant circuit (denoted by c for coolant) and (2) the CHP plant's heating water circuit (denoted by w for water). Figure 2 illustrates the model layout.

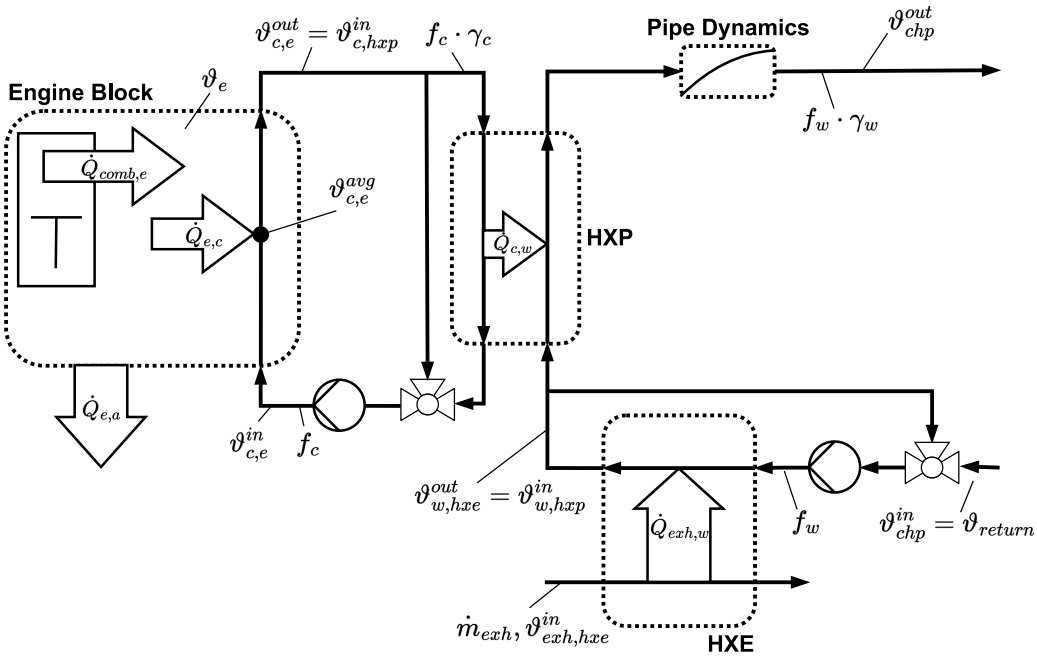

Figure 2. Simplified model overview.

3.3. Actuators

The actuators of our system are the two centrifugal pumps and the two three-way valves. Each centrifugal pump directly controls the main mass flow of the respective circuit, which are denoted by f_c for the coolant circuit and f_w for the heating water circuit. The positions of the three-way valves split these mass flows with certain split factors, denoted by γ_c and γ_w, respectively, each of which defines how much of the corresponding mass flow passes through the interconnecting HXP or bypasses it.

To achieve the targeted formulation of the mathematical optimization problem, we assume that the dynamics of the actuators can be neglected and that they are ideally controlled and can maintain their setpoints perfectly. This simplification allows us to treat both the main mass flows f_c and f_w and the two split factors γ_c and γ_w as control inputs. Once certain trajectories for these input variables are defined by the solution of the optimization problem, the actual control variables required by the physical actuators can be obtained via predefined feed-forward maps and tracked with simple Single-Input Single-Output (SISO) controllers such as PI controllers.

The mass flows in the coolant circuit are as follows:

$$\begin{aligned} f_{c,hxp}(t) &= \gamma_c(t) \cdot f_c(t) \\ f_{c,byp}(t) &= (1 - \gamma_c(t)) \cdot f_c(t) \end{aligned} \tag{1}$$

The mass flows in the water circuit are as follows:

$$\begin{aligned} f_{w,hxp}(t) &= \gamma_w(t) \cdot f_w(t) \\ f_{w,byp}(t) &= (1 - \gamma_w(t)) \cdot f_w(t) \end{aligned} \tag{2}$$

Assuming ideal mixing, the temperatures downstream of the valves thus follow as:

$$\begin{aligned} \vartheta_{c,e}^{in}(t) &= \gamma_c(t) \cdot \vartheta_{c,hxp}^{out}(t) + (1 - \gamma_c(t)) \cdot \vartheta_{c,e}^{out}(t) \\ \vartheta_{w,hxe}^{in}(t) &= \gamma_w(t) \cdot \vartheta_{chp}^{in}(t) + (1 - \gamma_w(t)) \cdot \vartheta_{w,hxe}^{out}(t) \end{aligned} \tag{3}$$

3.4. Reservoirs

The model of the CHP plant consists of four reservoirs, i.e., the engine block, the plate heat exchanger (HXP), the heat exchanger exhaust gas (HXE), and a supply pipe that feeds the heating water to the TES. They are visually marked by dashed outlines in Figure 2.

3.4.1. Engine

The engine block has the state variable ϑ_e, and the corresponding Ordinary Differential Equation (ODE) reads as:

$$m_e \, c_{p,e} \cdot \frac{\mathrm{d}}{\mathrm{d}t} \, \vartheta_e(t) = \dot{Q}_{comb,e} - \dot{Q}_{e,c}(t) - \dot{Q}_{e,a}(t) \tag{4}$$

The engine block and cylinder wall are lumped into a single component with mass m_e and specific heat capacity $c_{p,e}$.

For simplicity, this lumped element is referred to as the engine block. The heat flow due to combustion $\dot{Q}_{comb,e}$ is treated as constant due to the assumption of a constant mass flow of the air/fuel mixture (Section 3.2). The heat flow from the engine block to the coolant fluid $\dot{Q}_{e,c}$ is calculated by

$$\dot{Q}_{e,c}(t) = UA_{e,c} \cdot (\vartheta_e(t) - \vartheta_{c,e}^{avg}(t)), \tag{5}$$

where $UA_{e,c}$ is a lumped constant resulting from the heat transfer coefficient and the area of heat transfer and $\vartheta_{c,e}^{avg}$ is the temperature state of the coolant inside the engine. It is constructed as the arithmetic mean of the coolant temperatures at the engine's inlet and outlet. The heat flow from the engine block to the ambient $\dot{Q}_{e,a}$ is calculated by

$$\dot{Q}_{e,a}(t) = UA_{e,a} \cdot (\vartheta_e(t) - \vartheta_{air}), \tag{6}$$

where $UA_{e,a}$ is a lumped constant resulting from the convective heat transfer coefficient and the area of heat transfer to the ambient. $\vartheta_{c,e}^{avg}(t)$ is as in (5) and the corresponding ODE reads as:

$$m_{c,e} \, c_{p,c} \cdot \frac{\mathrm{d}}{\mathrm{d}t} \, \vartheta_{c,e}^{avg}(t) = \dot{Q}_{e,c}(t) - f_c(t) \, c_{p,c} \cdot (\vartheta_{c,e}^{out}(t) - \vartheta_{c,e}^{in}(t)), \tag{7}$$

with $m_{c,e}$ as the mass of coolant fluid inside the engine, $c_{p,c}$ the specific heat capacity of the coolant fluid, f_c the mass flow of the coolant fluid through the engine, and $\vartheta_{c,e}^{in}$ and $\vartheta_{c,e}^{out}$ as the temperatures at the engine's inlet and outlet, respectively.

3.4.2. Plate Heat Exchanger

There is a wealth of literature on the modeling of heat exchangers in hydraulic applications, e.g., [33–37]. In line with our application in an optimization context as well as our modeling principles (see Section 3.2) that require the model to be highly flexible, expandable with low complexity, and thus with little effort for parameter identification, we model the plate heat exchanger as a series of cells in each fluid path. Figure 3 illustrates the approach with two cells for each side. Each cell is assumed to be a stirred tank reactor. The temperature inside a cell is thus assumed to be equal to the temperature of the fluid flowing out of that cell. The corresponding symbols for the hot fluid entering and exiting a certain cell i are denoted by $\vartheta_{hot,i}^{in}$ and $\vartheta_{hot,i}^{out}$, respectively. The same principle applies to the cold fluid. The respective heat capacities c_p and the active heat exchange surface A, as well as the heat transfer coefficient k, are also assumed to be constant. The mass of the fluid and the corresponding mass flow are denoted by m and $\dot{m}$, respectively. Equations (8) and (9) describe the hot (Figure 3, left) and the cold (Figure 3, right) sides of the heat exchanger, respectively. Equation (10) describes the heat transfer between the hot side and the cold side and thus links the two differential equations. Note that the heat exchanger configuration is a counter-flow arrangement.

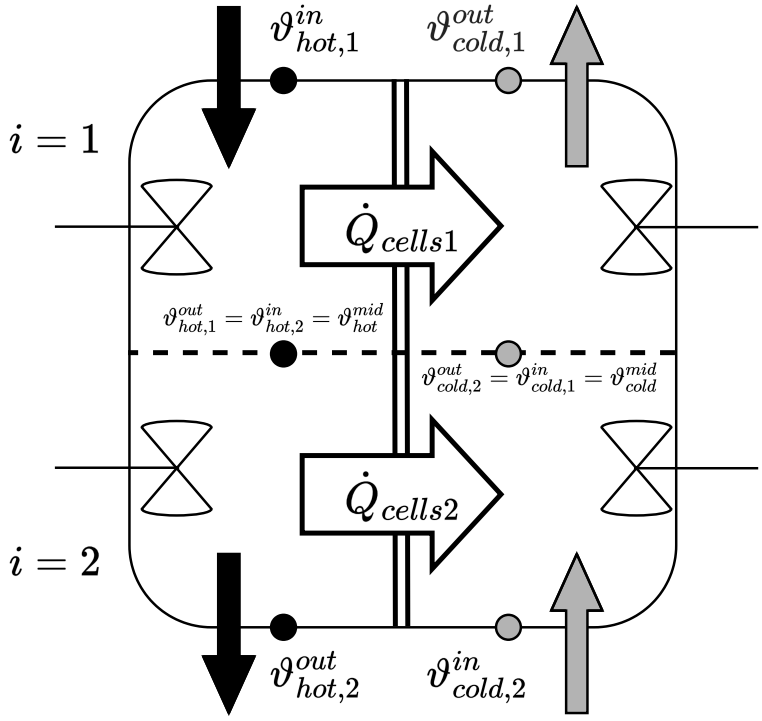

Figure 3. Heat Exchanger with $n_{cells} = 2$ for each fluid path.

The heat transfer equations for a generic single-cell setup are

$$m_{hot} c_{p,hot} \frac{\mathrm{d}}{\mathrm{d}t} \vartheta^{out}_{hot} = \dot{m}_{hot} c_{p,hot} (\vartheta^{in}_{hot} - \vartheta^{out}_{hot}) - \dot{Q}, \tag{8}$$

$$m_{cold} c_{p,cold} \frac{\mathrm{d}}{\mathrm{d}t} \vartheta^{out}_{cold} = \dot{m}_{cold} c_{p,cold} (\vartheta^{in}_{cold} - \vartheta^{out}_{cold}) + \dot{Q}, \tag{9}$$

$$\dot{Q} = kA(\vartheta^{out}_{hot} - \vartheta^{out}_{cold}). \tag{10}$$

Applying (8)–(10) on a heat exchanger with a total number of cells n_{cells}, the ODE of each single cell i yields:

$$\frac{\mathrm{d}}{\mathrm{d}t} \vartheta^{out}_{hot,i} = n_{cells} \frac{\dot{m}_{hot}}{m_{hot}} (\vartheta^{out}_{hot,i-1} - \vartheta^{out}_{hot,i}) - \frac{kA}{m_{hot}\, c_{p,hot}} (\vartheta^{out}_{hot,i} - \vartheta^{out}_{cold,i}), \tag{11}$$

$$\frac{\mathrm{d}}{\mathrm{d}t} \vartheta^{out}_{cold,i} = n_{cells} \frac{\dot{m}_{cold}}{m_{cold}} (\vartheta^{out}_{cold,i+1} - \vartheta^{out}_{cold,i}) + \frac{kA}{m_{cold}\, c_{p,cold}} (\vartheta^{out}_{hot,i} - \vartheta^{out}_{cold,i}). \tag{12}$$

The above formulation is highly flexible because the number of cells can be quickly decreased or increased to best adapt the model precision to the respective requirements. We iteratively determined that in the context of our modeling principles and precision requirements, $n_{cells} = 2$ is a suitable choice. Applying (11)–(12) to the original problem, the state equations for the coolant fluid (hot) read as:

$$\frac{\mathrm{d}}{\mathrm{d}t}\,\vartheta^{mid}_{c,hxp}(t) = 2\,\frac{f_c(t)\cdot\gamma_c(t)}{m_{c,hxp}}\left(\vartheta^{in}_{c,hxp}(t) - \vartheta^{mid}_{c,hxp}(t)\right) - \frac{kA_{hxp}}{m_{c,hxp}\,c_{p,c}}\left(\vartheta^{mid}_{c,hxp}(t) - \vartheta^{out}_{w,hxp}(t)\right), \tag{13}$$

$$\frac{\mathrm{d}}{\mathrm{d}t}\,\vartheta^{out}_{c,hxp}(t) = 2\,\frac{f_c(t)\cdot\gamma_c(t)}{m_{c,hxp}}\left(\vartheta^{mid}_{c,hxp}(t) - \vartheta^{out}_{c,hxp}(t)\right) - \frac{kA_{hxp}}{m_{c,hxp}\,c_{p,c}}\left(\vartheta^{out}_{c,hxp}(t) - \vartheta^{mid}_{w,hxp}(t)\right). \tag{14}$$

Similarly, the state equations for the water side (cold) follow as:

$$\frac{\mathrm{d}}{\mathrm{d}t}\,\vartheta^{out}_{w,hxp}(t) = 2\,\frac{f_w(t)\cdot\gamma_w(t)}{m_{w,hxp}}\left(\vartheta^{mid}_{w,hxp}(t) - \vartheta^{out}_{w,hxp}(t)\right) + \frac{kA_{hxp}}{m_{w,hxp}\,c_{p,w}}\left(\vartheta^{mid}_{c,hxp}(t) - \vartheta^{out}_{w,hxp}(t)\right), \tag{15}$$

$$\frac{\mathrm{d}}{\mathrm{d}t}\,\vartheta^{mid}_{w,hxp}(t) = 2\,\frac{f_w(t)\cdot\gamma_w(t)}{m_{w,hxp}}\left(\vartheta^{in}_{w,hxp}(t) - \vartheta^{mid}_{w,hxp}(t)\right) + \frac{kA_{hxp}}{m_{w,hxp}\,c_{p,w}}\left(\vartheta^{out}_{c,hxp}(t) - \vartheta^{mid}_{w,hxp}(t)\right). \tag{16}$$

Note that we used the previously introduced notation f for the main circuit mass flows and the indices c for the coolant fluid and w for the water circuit.

3.4.3. Exhaust Gas Heat Exchanger

The key advantage of the modeling approach for the plate heat exchanger is that it is generic in the description of the heat transfer and can therefore be applied to any other sort of heat exchanger. We therefore use the same modeling approach for the HXE as for the HXP described in Section 3.4.2, despite the HXE being a shell-and-tube heat exchanger with gas-to-water heat transfer. It is also set up in a counter-flow arrangement. However, for reasons of simplicity, we do not model the engine's exhaust manifold, the exhaust dynamics in the exhaust pipe, or the TWC, as this would directly oppose our modeling principles discussed in Sections 3.1 and 3.2. Instead, we set both the exhaust gas temperature entering the heat exchanger and the corresponding exhaust gas mass flow as constant. This simplification does not hold for the entire operating time under steady-state conditions. However, we found that, during the short time span of a start-up, the TWC acts as such a large inertia that the identification of a constant exhaust gas temperature and mass flow upstream of the heat exchanger results in only small variations in the relevant water outlet temperature. With these assumptions, the state equations are constructed similarly to equations in the HXP case and read as:

$$\frac{\mathrm{d}}{\mathrm{d}t}\,\vartheta^{mid}_{exh,hxe}(t) = 2\,\frac{\dot{m}_{exh}}{m_{exh,hxe}}\left(\vartheta^{in}_{exh,hxe} - \vartheta^{mid}_{w,hxe}(t)\right) - \frac{kA_{hxe}}{m_{exh,hxe}\,c_{p,exh}}\left(\vartheta^{mid}_{exh,hxe}(t) - \vartheta^{out}_{w,hxe}(t)\right), \tag{17}$$

$$\frac{\mathrm{d}}{\mathrm{d}t}\,\vartheta^{out}_{exh,hxe}(t) = 2\,\frac{\dot{m}_{exh}}{m_{exh,hxe}}\left(\vartheta^{mid}_{exh,hxe}(t) - \vartheta^{out}_{exh,hxe}(t)\right) - \frac{kA_{hxe}}{m_{exh,hxe}\,c_{p,exh}}\left(\vartheta^{out}_{exh,hxe}(t) - \vartheta^{mid}_{w,hxe}(t)\right), \tag{18}$$

where $\dot{m}_{exh}$ is the constant exhaust gas mass flow, $c_{p,exh}$ is the specific heat capacity of the exhaust gas, m_{exh} is the constant exhaust gas mass inside the HXE, and $\vartheta^{in}_{exh,hxe}$ is the constant exhaust gas temperature during start-up.

Similarly, the state equations for the water side read as:

$$\begin{aligned}\frac{\mathrm{d}}{\mathrm{d}t}\,\vartheta^{out}_{w,hxe}(t) = 2\,\frac{f_w(t)}{m_{w,hxe}}\Big(\vartheta^{mid}_{w,hxe}(t) - \vartheta^{out}_{w,hxe}(t)\Big) \\ + \frac{kA_{hxe}}{m_{w,hxe}\,c_{p,w}}\Big(\vartheta^{mid}_{exh,hxe}(t) - \vartheta^{out}_{w,hxe}(t)\Big),\end{aligned} \tag{19}$$

$$\begin{aligned}\frac{\mathrm{d}}{\mathrm{d}t}\,\vartheta^{mid}_{w,hxe}(t) = 2\,\frac{f_w(t)}{m_{w,hxe}}\Big(\vartheta^{in}_{w,hxe}(t) - \vartheta^{mid}_{w,hxe}(t)\Big) \\ + \frac{kA_{hxe}}{m_{w,hxe}\,c_{p,w}}\Big(\vartheta^{out}_{exh,hxe}(t) - \vartheta^{mid}_{w,hxe}(t)\Big).\end{aligned} \tag{20}$$

3.4.4. Dynamics of Water Supply Pipe

It is often the case that the supply pipe, which delivers the heating water supply to a TES or any other system component, has a considerable length. We account for the associated dynamics by including a thermal inertia downstream of the HXP. The corresponding ODE reads as:

$$m_{w,supply}\cdot\frac{\mathrm{d}}{\mathrm{d}t}\,\vartheta^{out}_{chp}(t) = f_w(t)\cdot\gamma_w(t)\cdot(\vartheta^{out}_{w,hxp}(t) - \vartheta^{out}_{chp}(t)). \tag{21}$$

3.5. Model Validation

We determined the model parameters by means of a parameter identification on the mCHP test rig. The complete set of estimated parameters is listed in Appendix A.

Figure 4 (left) illustrates the measurement for a warm-up procedure on the mCHP test rig without any valve actuation, i.e., no flow occurs in the bypass of each hydraulic circuit. In the following, this case is referred to as the reference case. The time from start-up to reaching $\vartheta^{out}_{chp} = 80\,°\mathrm{C}$ is about $t = 14.7\,\mathrm{min}$. This case is a warm-up process with all relevant system temperatures initialized at $\vartheta = 20\,°\mathrm{C}$. The desired heating water temperature in a steady-state operation is $\vartheta^{out}_{ref} = 80\,°\mathrm{C}$. The reference warm-up is based on heat-led control of the centrifugal pumps via PI controllers with both three-way valves fully opened, i.e., $\gamma_c = \gamma_w = 1$. The return temperature is kept at $\vartheta^{in}_{chp} = 30\,°\mathrm{C}$ by an external controller. Furthermore, the centrifugal pump in the coolant circuit of the engine controls the temperature difference between the inlet and outlet to $\Delta\vartheta_{c,e} = 5\,°\mathrm{C}$, whereas the centrifugal pump in the heating circuit is operated at minimum speed during the warm-up phase, i.e., $f_w = 0.15\cdot f_{w,max}$. The model can accurately represent this warm-up. This was to be expected as valves are constantly fully opened and the pumps are set to a constant so that no significant mass flow dynamics occur. In contrast, Figure 4 (right) illustrates a warm-up with considerable actuation. The temperatures at the engine outlet $\vartheta^{out}_{c,e}$ and the mCHP outlet ϑ^{out}_{chp} still closely match the measurement. In total, we conducted ten validation measurements with different rates and levels of actuation. Given the substantial simplifications, we conclude that the model adequately reflects the plant's responses to varying actuator inputs.

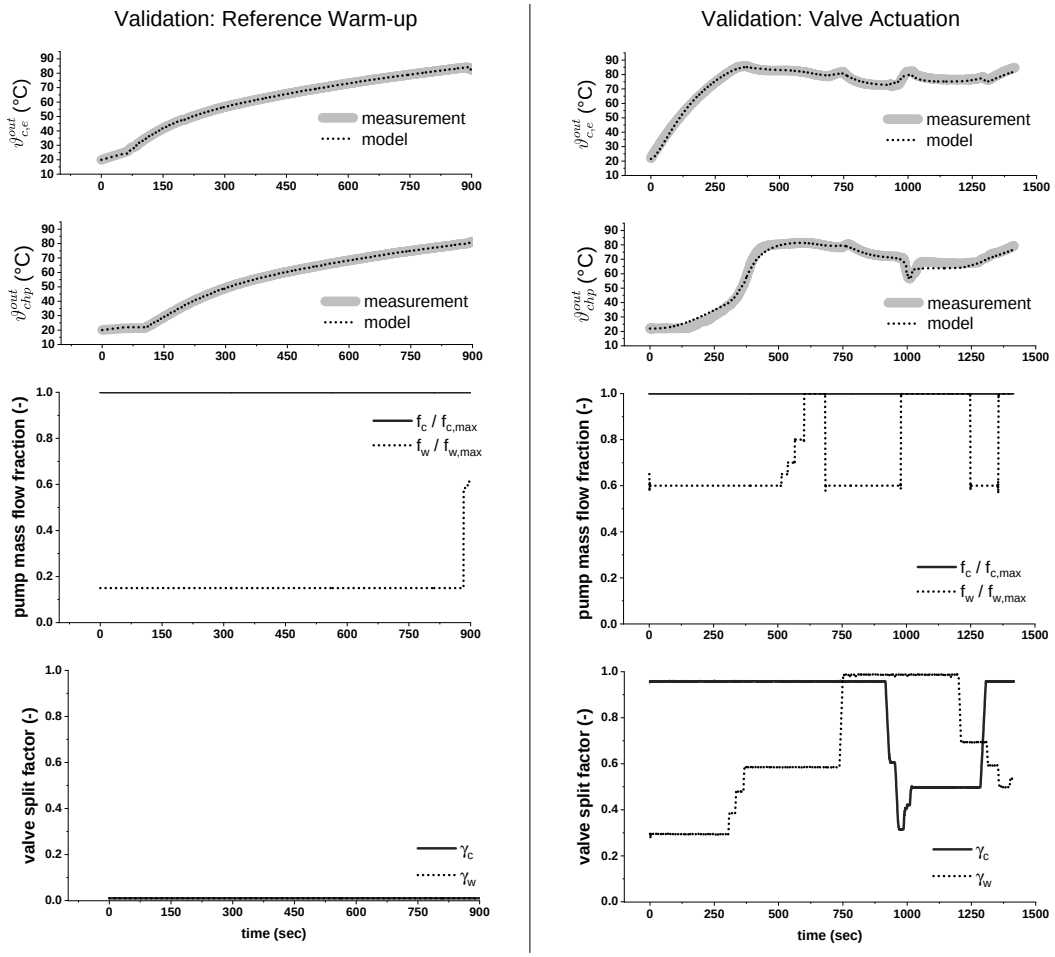

Figure 4. Comparison of model behavior with reference measurement (**left**) and warm-up measurement with significant actuation (**right**).

4. Optimization

In this section, the formulation of the mathematical optimization problem is presented. Therefore, we adopt the model equations presented in Section 3 above and translate them into a set of decision variables, constraints, and an objective function. The resulting Optimal Control Problem (OCP) is implemented in Matlab as a Nonlinear Program (NLP) via the CasADi interface [38]. The problem is solved by Ipopt [39] and the linear solver MUMPS [40].

For the transcription of the mathematical model, we discretize the ODEs based on the forward Euler method and adopt the direct multiple shooting approach [41], where the continuity of the state variables is ensured via so-called gap closing constraints. As a result, the exemplary ODE $\dot{x}(t) = f(x(t), u(t))$ is implemented as a set of $N-1$ equality constraints as follows:

$$x[k+1] = x[k] + T_s \cdot f\big(x[k], u[k]\big) \qquad \forall k = 1, \ldots, N-1, \tag{22}$$

where k is the discrete time index and T_s is the uniform time period between consecutive samples. The square brackets are used to indicate discrete-time vector elements, compared to the parentheses for arguments of continuous-time functions. Due to the non-convexity of the overall OCP, we acknowledge that local optima might exist, and therefore do not claim global optimality within this study.

4.1. Constraints

To implement the model from Section 3, we utilize (22) to transcribe (3), (4), (7), and (13)–(21). To further ensure the integrity of our model the following identities are always in place. They are also indicated in Figure 2. The temperature of the cooling water exiting the engine is equal to the temperature entering the plate heat exchanger, i.e.,

$$\vartheta_{c,e}^{out}[k] = \vartheta_{c,hxp}^{in}[k] \qquad \forall k = 1, \dots, N. \tag{23}$$

The temperature of the heating water exiting the HXE is equal to the temperature entering the HXP, i.e.,

$$\vartheta_{w,hxp}^{in}[k] = \vartheta_{w,hxe}^{out}[k] \qquad \forall k = 1, \dots, N. \tag{24}$$

Furthermore, we ensure that the following physical boundaries are met at all times. The difference between the temperatures of the coolant entering the engine and leaving the engine is kept below a certain threshold value in order to prevent stress cracks in the engine block. We therefore set

$$\vartheta_{c,e}^{out}[k] - \vartheta_{c,e}^{in}[k] \leq \Delta\vartheta_{c,e,max} \qquad \forall k = 1, \dots, N. \tag{25}$$

Hence, in order to emulate the dynamical behavior of the pumps and valves, respectively, we further constrain the change rates of the mass flows controlled by both centrifugal pumps and the split factors of both three-way valves, yielding:

$$-\dot{f}_{x,max} \leq \frac{f_x[k+1] - f_x[k]}{T_s} \leq \dot{f}_{x,max} \qquad \forall k = 1, \dots, N-1 \tag{26}$$

$$-\dot{\gamma}_{x,max} \leq \frac{\gamma_x[k+1] - \gamma_x[k]}{T_s} \leq \dot{\gamma}_{x,max} \qquad \forall k = 1, \dots, N-1 \tag{27}$$

with $x \in \{c, w\}$ for cooling and heating circuit, respectively. Finally, the temperature state of the coolant inside the engine introduced in (5) is defined to be the arithmetic mean of the temperature entering and exiting the engine,

$$\vartheta_{c,e}^{avg}[k] = \frac{\vartheta_{c,e}^{in}[k] + \vartheta_{c,e}^{out}[k]}{2} \qquad \forall k = 1, \dots, N. \tag{28}$$

4.2. Objective

The main purpose of our optimization problem is to find quick warm-up strategies, an objective that is not simple to implement within the proposed time discretization in (22). Therefore, we use a workaround by adding an additional condition to the problem that forces the warm-up phase to be completed after a certain time, and then we repeatedly reduce this time and continue to solve the problem until it is no longer feasible. The last feasible solution is the one we are looking for. Of course, there are many other search algorithms that are applicable here, such as the bracketing method.

The additional condition mentioned above is implemented as the following inequality constraint

$$\vartheta_{chp}^{out}[k] \geq \vartheta_{ref}^{out} \qquad \forall k \geq k^\star, \tag{29}$$

where $k^\star$ represents the point in time $t^\star = k^\star \cdot T_s$ from which the desired temperature ϑ_{chp}^{out} of the water supplied by the CHP is guaranteed to be at least at the reference ϑ_{ref}^{out}. For numerical stability, we formulate the objective of our OCP as follows:

$$\min \quad T_s \sum_{k=k^\star}^{N} (\vartheta_{chp}^{out}[k] - \vartheta_{ref}^{out})^2, \tag{30}$$

where $k^\star$ is again predefined for each iteration as described above. This formulation minimizes the sum of squared temperature deviations at $k \in \{k^\star, \dots, N\}$ only instead of along the entire horizon, which offers the optimization as much freedom as possible in how it arrives there.

To obtain actuator and state trajectories of the system beyond the warm-up phase, we chose a time horizon that is 2 min longer than $t^\star$. We further set $T_s = 2\,\mathrm{s}$, which in our experience represents a good balance between accuracy and computational efficiency. Still, due to the computational effort caused by the iterative nature, we see this method, at least in its current rudimentary implementation, as being suitable mainly for offline optimizations. For example, for creating reference trajectories, comparing system designs and control strategies, or gaining a deeper understanding of optimal warm-up strategies.

4.3. Further Variants of Objectives

The objective in Section 4.2 is mostly intuitive, as we aim to reach a defined steady-state temperature as quickly as possible. However, many further cost functions can be implemented in a straightforward fashion, depending on the respective physical priorities. To showcase the flexibility of our framework we include two cost function variants in the following considerations, while the one introduced above in (30) is denoted by Temperature Deviation for clarity.

The first variant prioritizes heating up the engine. As soon as the engine has reached the steady-state reference temperature, the objective changes to raise the supply temperature as quickly as possible. This variant thus accounts for the fact that the engine is the main source of heat energy that is being transferred to the heating water circuit during warm-up conditions. As a further benefit, a quick warm-up of the engine also means a rapid warm-up of the engine oil, which has a favorable effect on durability. This variant is thus further denoted by Durability. The associated objective function reads as

$$\min \quad \sum_{k=\hat{k}}^{N} (\vartheta_{chp}^{out}[k] - \vartheta_{ref}^{out})^2, \tag{31}$$

where $\hat{k} \in 1, \dots, N$ is the earliest point in time at which $\vartheta_{c,e}^{out}[k] = \vartheta_{ref}^{out}$ is reached.

The index $\hat{k}$ is constructed via a pre-simulation with a closed coolant valve, i.e., $\gamma_c = 0$. We further note that we use the temperature exiting the engine in this case, as this is the relevant temperature for the heat transfer to the heating water via the plate heat exchanger.

The second variant connects to the statement of Section 1 that the warm-up phase is characterized by a low total efficiency due to the almost complete lack of thermal efficiency. In this variant, we therefore formulate the objective so that the thermal efficiency during warm-up is maximized. An adequate measure is given by

$$\eta_{th} = \frac{f_w \cdot \gamma_w \cdot c_{p,w} \cdot (\vartheta_{chp}^{out} - \vartheta_{chp}^{in})}{\dot{Q}_{comb,e}}, \tag{32}$$

where the time dependence is omitted for clarity. Since the supplied combustion heat $\dot{Q}_{comb,e}$, the specific heat capacity $c_{p,w}$, and the return temperature ϑ_{chp}^{in} are all treated as constant, we can simplify the corresponding objective function to

$$\max \quad \sum_{k=1}^{N} \vartheta_{chp}^{out}[k] \cdot f_w[k] \cdot \gamma_w[k]. \tag{33}$$

This variant is further denoted by Efficiency.

5. Case Study

In this section, we present eight cases listed in Table 1 that illustrate the versatility and flexibility of our proposed framework. Each case is associated with one of the three priorities

and their corresponding cost functions presented in Section 4.3. For a fair comparison of their performance, the time from which the temperature ϑ_{chp}^{out} must be at least be 80 °C is set to the smallest possible value that is feasible for all of them. For the corresponding cases ①, ②, and ③, this shortest warm-up time is found to be $t^\star = 580\,\mathrm{s}$, imposed by case ③ representing the priority Thermal Efficiency. This warm-up time already represents a reduction of about 34% compared to the measured reference case in Section 3.5.

As $t^\star = 580\,\mathrm{s}$ is not the minimal warm-up time for the priorities Temperature Deviation and Durability, their time-optimal cases are represented by ④ and ⑤ with the corresponding warm-up times $t^\star = 538\,\mathrm{s}$ and $t^\star = 560\,\mathrm{s}$, respectively.

To shed light on the influence of the system-specific actuator constraints on the solution of the OCP, we revisit cases ① to ③ as cases ⑥ to ⑧, respectively, but omit the actuator constraints (26) and (27).

Table 1. Case overview.

No.	Priority	Objective	$t^\star$	Constraints
①	Temperature Deviation	Equation (30)	580 s	Equations (3), (4), (7), (13)–(21), (23)–(29)
②	Durability	Equation (31)	580 s	Equations (3), (4), (7), (13)–(21), (23)–(29)
③	Thermal Efficiency	Equation (33)	580 s	Equations (3), (4), (7), (13)–(21), (23)–(29)
④	Temperature Deviation (time optimal)	see ①	538 s	Equations (3), (4), (7), (13)–(21), (23)–(29)
⑤	Durability (time optimal)	see ②	560 s	Equations (3), (4), (7), (13)–(21), (23)–(29)
⑥	Temperature Deviation (no input constraints)	see ①	580 s	Equations (3), (4), (7), (13)–(21), (23)–(25), (28)–(29)
⑦	Durability (no input constraints)	see ②	580 s	Equations (3), (4), (7), (13)–(21), (23)–(25), (28)–(29)
⑧	Thermal Efficiency (no input constraints)	see ③	580 s	Equations (3), (4), (7), (13)–(21), (23)–(25), (28)–(29)

Figure 5 directly contrasts cases ①–③ by means of two temperature curves: the main temperature of interest ϑ_{chp}^{out} and the temperature of the coolant exiting the engine $\vartheta_{c,e}^{out}$. The latter is listed to better illustrate the heat transfer across the plate heat exchanger, as both the hot side inlet temperature and the cold side outlet temperature are shown. In addition, the mass flows resulting from solving the optimization problem are listed for each case. Following our modeling approach in Section 3, the valve inputs precisely represent a split factor that only forms a mass flow in combination with the associated pump input.

For case ①, Figure 5 suggest that the optimal temperature curve for ϑ_{chp}^{out} closely follows the temperature curve of $\vartheta_{c,e}^{out}$, with a difference of about $\Delta\vartheta = 10\,°\mathrm{C} - 12\,°\mathrm{C}$ for a large part of the warm-up process. The optimal characteristic for $\vartheta_{c,e}^{out}$ consists of reaching a temperature level well above the steady-state reference temperature shortly before $t^\star$. This strategy enables the water pump and valve, or f_w and γ_w as their equivalents in the optimization, to ramp up the mass flow through the HXP and increase the heat transferred from the cooling to the water circuit. This quickly bridges the gap between $\vartheta_{c,e}^{out}$ and ϑ_{chp}^{out} such that the latter rises above the steady-state reference of 80 °C at $t^\star = 580\,\mathrm{s}$. In turn, $\vartheta_{c,e}^{out}$ decreases due to the elevated heat transfer. If $\vartheta_{c,e}^{out}$ were to drop below the reference temperature, ϑ_{chp}^{out} would inevitably follow with a certain time delay. To prevent this, the optimizer reduces the coolant mass flow through the HXP by reducing the split factor γ_c, thereby effectively dampening the effect on $\vartheta_{c,e}^{out}$. Furthermore, it can be noted that the optimization keeps the main coolant mass flow f_c as the equivalent of the coolant pump actuator approximately constant. This is largely due to the constraint in (25) that limits the coolant temperature difference across the engine.

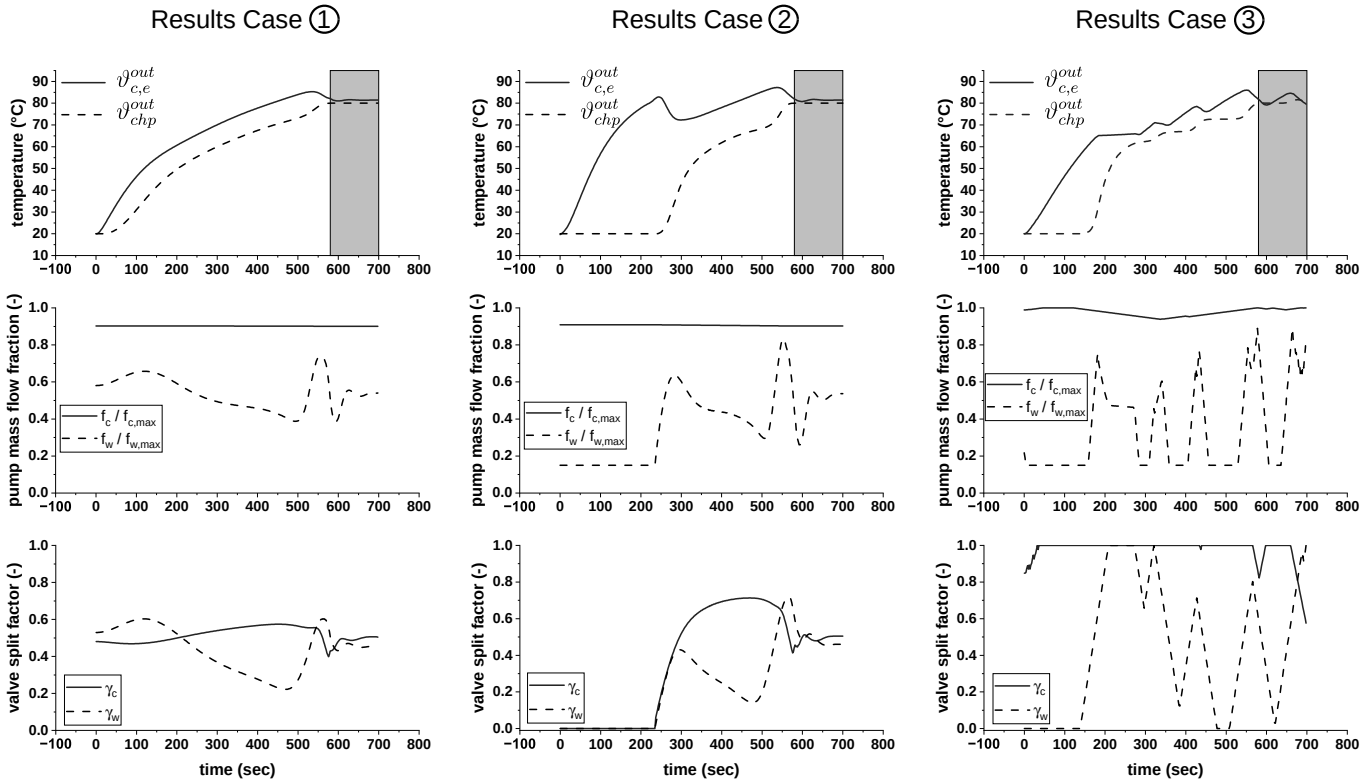

Figure 5. Comparison of cases ① (**left**), ② (**middle**), and ③ (**right**) for $t^\star = 580\,\mathrm{s}$.

In light of the observation that during warm-up conditions $\vartheta^{out}_{c,e}$ represents the main source of thermal energy, case ② can be considered as an intuitive warm-up strategy. Here, $t^\star = 580\,\mathrm{s}$ as in case ①. However, Figure 5 shows that the slightly different objective leads to different key characteristics. As the priority is to bring $\vartheta^{out}_{c,e}$ into line with the reference temperature, the optimizer closes both valves or sets both split factors f_c and f_w to zero, such that no heat transfer via the HXP is possible. Once $\vartheta^{out}_{c,e}$ reaches the steady-state reference temperature, the control strategy raises ϑ^{out}_{chp} to 80 °C. As a result, heat is transferred from the cooling circuit to the water circuit. The mass flow f_w and the split factors γ_c and γ_w are therefore increased. Subsequently, $\vartheta^{out}_{c,e}$ drops below the reference temperature. However, in this particular situation the optimal strategy is to decrease f_w and γ_w, i.e., the mass flow of the heating water through HXP $f_w \cdot \gamma_w$, instead of γ_c. This behavior can be attributed to the large temperature difference between $\vartheta^{out}_{c,e}$ and ϑ^{out}_{chp}. To achieve the objective, it is optimal to slowly decrease the mass flow $f_w \cdot \gamma_w$. Consequently, both temperatures rise. Shortly before $t^\star = 580\,\mathrm{s}$, the engine temperature is well above the reference temperature such that the mass flows of both the pump and the valve of the water circuit are sharply increased to raise ϑ^{out}_{chp} to reference temperature levels. Similar to case ①, γ_c is actuated here to prevent $\vartheta^{out}_{c,e}$ from dropping below the reference temperature, as this would lead ϑ^{out}_{chp} to do the same and violate (29). Furthermore, f_c is also used here to limit the coolant temperature difference across the engine, which indicates that the influence on optimizing the warm-up process is negligible.

Case ③ shows a different characteristic than the two previous cases. Here, the warm-up strategy is actually time-optimal, as values smaller than $t^\star = 580\,\mathrm{s}$ render the optimization problem infeasible. Following Section 4.3, the objective is to maximize the thermal efficiency over the entire horizon while reaching $\vartheta^{out}_{chp} = 80\,°\mathrm{C}$ at $t^\star$. The temperature trajectories shown in Figure 5 share similarities with those in case ②, e.g., the engine is heated up first, the heating water valve is closed ($\gamma_w = 0$), and the heating water pump is kept at minimum speed ($f_w = 0.15$). However, f_c and γ_c are at their maximum for large parts of the entire warm-up process. This measure once again aims to limit the coolant

temperature difference across the engine. The optimal strategy also takes advantage of γ_c in this case because both the water pump and valve, i.e., f_w and γ_w, are actuated with high rates, which has a large impact on the temperature difference. The settings of the heating water mass flows are a direct result of the cost function in (33) since the product of both control inputs and the main CHP temperature ϑ_{chp}^{out} is maximized. From a strategic point of view, in case ③, the temperature $\vartheta_{c,e}^{out}$ is first increased, although not up to reference temperature as in case ②. Subsequently, the mass flow through HXP, i.e., the product of $f_w \cdot \gamma_w$, is strongly increased, such that the CHP temperature ϑ_{chp}^{out} approaches $\vartheta_{c,e}^{out}$. Before $\vartheta_{c,e}^{out}$ starts to decrease due to the high heat flow to the water circuit, the mass flow $f_w \cdot \gamma_w$ is again decreased at a high rate. This is followed by a phase in which the mass flow alternately increases and decreases, which results in an increase-and-hold pattern of ϑ_{chp}^{out} until the reference temperature is reached at time $t^\star$.

The previous considerations are limited to the comparison to a uniform warm-up time $t^\star = 580\,\mathrm{s}$, which is determined according to the feasibility limit of case ③. Accordingly, the comparison of the respective time-optimal cases ④ and ⑤ is shown in Figure 6, where $t^\star = 538\,\mathrm{s}$ and $t^\star = 560\,\mathrm{s}$, respectively (see also Table 1). For case ④, except for the reduction in warm-up time, only marginal differences in the input trajectories from case ① can be observed. However, case ⑤ shows similar mass flow and split factor trajectories as case ③, despite the different objectives. This is due to the fact that in both cases, ϑ_{chp}^{out} is only raised once $\vartheta_{c,e}^{out}$ has reached a certain temperature level. The resulting input trajectories are thus optimal to rapidly increase ϑ_{chp}^{out} according to the rate constraints in (26) and (27) and with respect to $\vartheta_{c,e}^{out}$.

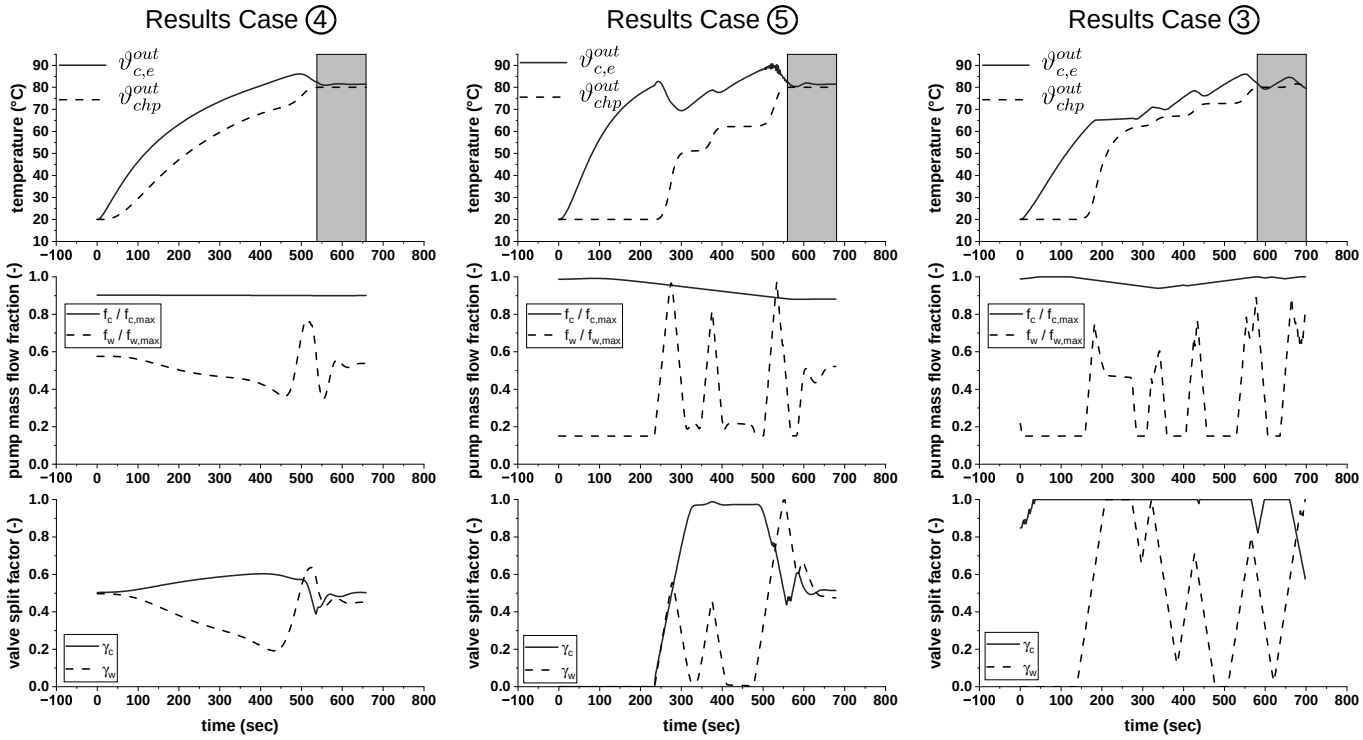

Figure 6. Comparison of time optimal cases ④ (**left**), ⑤ (**middle**), and ③ (**right**).

In contrast to the previous considerations, the proposed framework can also be used to investigate interdependencies that would otherwise be cumbersome or technically impossible to determine. Thus, Figure 7 illustrates cases ⑥–⑧, which are analogous with cases ①–③ presented in Figure 5, but with the difference being that the input rate constraints (26) and (27) are omitted.

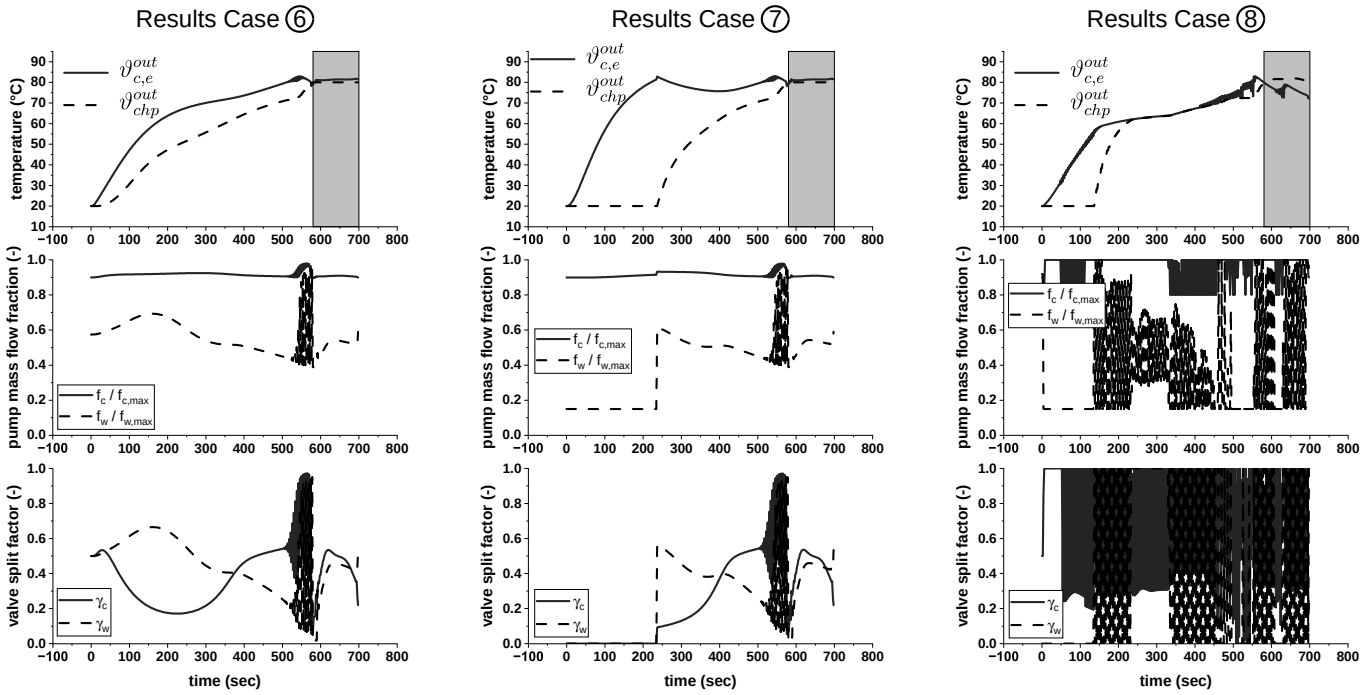

Figure 7. Comparison of case ⑥ (**left**), ⑦ (**middle**), and ⑧ (**right**) for $t^\star = 580\,\mathrm{s}$ with no input rate constraints (26) and (27).

Figure 7 illustrates that the pumped mass flows and the water valve split factor do not fundamentally change compared to cases ①, ② and ③. The high-rate actuation becomes even more prominent for "Thermal Efficiency" (case ⑧) and begins to also occur for ⑥ and ⑦ shortly before the reference temperature is reached. The main characteristics of these actuators, however, remain similar. The exception to this is the coolant split factor, particularly for cases ⑥ and ⑦. The lifted rate-constraint enables the optimizer to utilize the split factor of the coolant valve to generate a smoother heat-transfer via the plate heat exchanger. This in turn also results in a smoother characteristic of the output temperature ϑ_{chp}^{out}. This can be seen particularly well in cases ⑦ and ⑧ as an initially large temperature difference between $\vartheta_{c,e}^{out}$ and ϑ_{chp}^{out} is reduced until $t^\star = 580\,\mathrm{s}$. For cases ②, ③, and ⑤ the constraints (26) and (27) lead to a kind of plateau formation in phases of high-rate actuation (Figures 5 and 6).

6. Discussion

The case study in Section 5 provides a quick glimpse into the capabilities and the flexibility of the developed framework, as there are numerous possibilities for other objectives and constraints. From the small subset presented here, we can, however, note some key insights.

6.1. Key Insights

Supposing that time optimality is the primary concern, i.e., heating up to steady-state conditions should be as fast as possible, case ④ is the best choice. The optimized trajectories of the pump mass flows and valve split factors enable the shortest warm-up time, which is 39% smaller compared to the measured reference case with no valve actuation in Section 3.5. Case "Durability" (⑤) takes slightly longer, but ensures that the engine warm-up is prioritized first. The resulting benefits mainly concern the mechanical aspects of the plant, e.g., lubrication properties of the engine oil and lifetime of engine components and thus maintenance costs. Case "Thermal Efficiency" (③) takes longer than ④ (+7%) and ⑤ (+3%). However, $t^\star = 580\,\mathrm{s}$ still results in a total 34% reduction in warm-up time.

Now suppose that the warm-up phase and that thermal efficiency is the primary concern. By design, case ③ would be the best choice. However, comparing the remaining cases to case ③ in terms of their thermal efficiency is not intuitively straightforward. To allow for a fair comparison, we align the horizons of ④ and ⑤ to match ③, but keep $t^\star$ as listed in Table 1. As a result, Figure 8 shows that only case ① can keep up with a reduced efficiency of about 9%, whereas the efficiency of the corresponding time-optimal case ④ drops by about 21%.

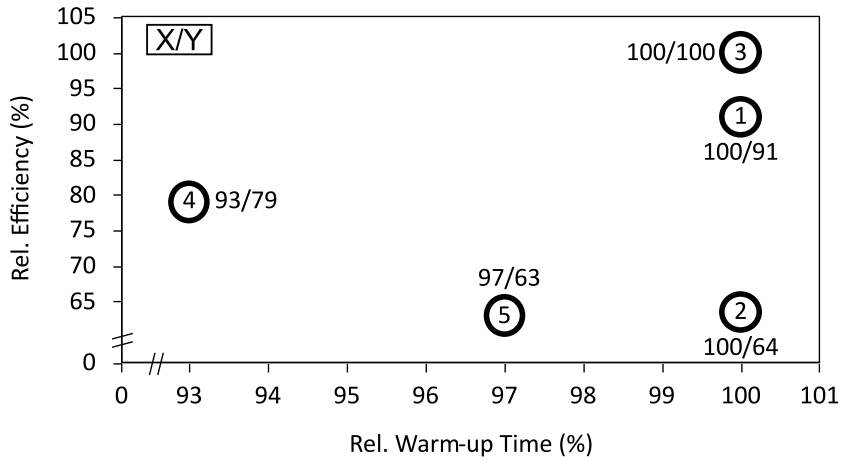

Figure 8. Case comparison based on relative efficiencies and warm-up times.

This result shows that a shorter warm-up phase cannot generally be associated with the best solution, particularly through the lens of maximizing the power output and, thus, efficiency. However, for the purpose of this case study, we put a time limit for the warm-up phase via (29) to ensure comparability of the various cases. If this constraint is lifted and the objective is replaced with one that respects both the time penalty and the efficiency (30) and (33), e.g., via the method of weighted sums [42,43], the optimization problem allows to systematically generate a Pareto front that evaluates the trade-off between warm-up time and thermal efficiency.

6.2. Limitations

The current setup of the optimization problem requires the explicit formulation of final state constraints on a fixed horizon, e.g., in our case reaching a reference temperature ϑ_{ref}^{out} after time $t^\star$. Additionally, as mentioned in Section 4, global optimality is not guaranteed due to the non-convexity of the mathematical model. However, in our experience, this has not proved to be relevant in practice. On the other hand, if the optimization framework is to be applied in an MPC-context, this property needs to be analyzed in detail. Then, the execution time becomes also critical and requires systematic improvement. Since this work provides a starting point for the improvement of the warm-up phase, we chose to focus on cold-starts. Hence, warm-up processes at different initial temperatures are left for future research. Finally, we restricted our analysis to a specific experimental mCHP plant. Hence, although the optimization framework is flexible and can be adapted to other systems, its practical applicability has yet to be demonstrated.

7. Implications and Future Application

Our results illustrate that mathematical optimization can help to significantly improve the warm-up behavior of an mCHP plant. The achieved increase in total efficiency and decrease in warm-up time enables future flexibility and more demand-driven operations. In the following, we shed light on the implications that can be drawn from this study and provide starting points for future developments.

7.1. Different Operating Conditions

For our study, we have set fixed operating conditions. This way, we can compare our results and effectively quantify different measures, e.g., different objective functions. Beyond that, different operating conditions can be investigated. For instance, the desired steady-state temperature can easily be adjusted via (29). The same applies for the return temperature and the initial temperatures. The latter provide the means of investigating the effect of different initial temperature levels on the optimal actuator trajectories and thus effectively allow for generating statements for warm-start conditions.

7.2. Demand-Side Interaction

In Section 2, we state that, for the purpose of this study, we set the system boundary to omit the demand side, illustrated in Figure 1 with a TES. A meaningful extension of this work could be to embed a model of the TES, where the storage temperature could serve as an additional decision variable in the optimization. Such a holistic approach would allow to incorporate possible physical boundary conditions of the TES, e.g., limits of the entering/exiting mass flows in stratified TES applications. Especially in the presence of frequent warm-up processes due to demand-driven operation, the additional benefit is expected to be significant.

However, our mCHP-system can also provide thermal energy directly to end-users as the output temperature can be effectively decoupled from the engine temperature due to the two three-way valves. Accordingly, further studies may focus on prediction methods, e.g., with gaussian processes, that estimate the demand of end-users and then adjust the constraints of the optimization problem before its execution.

7.3. Cost-Effectiveness

The CHP sector is tremendously cost-sensitive such that each measure must be evaluated against the costs incurred. Compared to conventional system layouts, our mCHP system utilizes two continuously adjustable three-way valves that allow for bypassing the central plate heat exchanger which links both hydraulic circuits. These valves enable us to demonstrate the impact of our optimization framework on the thermal warm-up behavior and the achievable performance increase. We are convinced that the achievable benefits in terms of energy savings outweigh the additional costs of integrating these valves.

7.4. Implementation

The optimization routine generates optimal time-based output trajectories for each actuator during the warm-up phase. One approach of realizing these trajectories consists of implementing PI controllers for the actuators, each of which aims to track the corresponding reference trajectory. Additionally, the decision variables do not directly describe the actuator control signals but physical quantities, mass flows and mass flow fractions, that are convenient for the model formulation. We have built predefined look-up tables that map our actuator inputs to these model quantities during the system identification process. These look-up tables can be inverted to translate the values of the optimized reference trajectories to appropriate actuator control signals in a feed-forward control fashion.

SISO approaches are not optimal in case of systemic cross-couplings. Therefore, the plant could be operated in an MPC-fashion [44] during the warm-up phase. The optimization problem would be solved repeatedly on a receding horizon, taking into account the current temperature and actuator values as initial conditions. This approach effectively handles any cross-couplings and disturbances.

8. Conclusions

The warm-up process is one of the main causes of inefficiency in the operation of an mCHP plant, so it is desirable to quickly reach steady-state operating conditions. In this study, we propose an optimization framework to improve the warm-up performance of an mCHP plant. The framework consists of an experimentally validated physics-based

model of a real-world mCHP plant and generates optimal time-based actuator trajectories. Selected case studies illustrate that the optimization result can lead to large improvements in the thermal behavior, e.g., up to a 40% shorter warm-up phase. These performance gains are achieved with only a small set of parameters and a model of low complexity. Utilizing the flexibility and versatility of the framework, we study various objectives and evaluate the trade-offs between the duration and the thermal efficiency of the warm-up phase. With a further expansion into an MPC control structure, the optimization framework presented in this work could make a significant contribution to increasing the efficiency of mCHP plants and to facilitating the wider adoption of this type of energy generation units.

Author Contributions: Conceptualization, T.Z., A.R. and C.H.O.; methodology, T.Z. and A.R.; software, T.Z. and A.R.; validation, T.Z. and A.R.; formal analysis, T.Z.; investigation, T.Z.; resources, T.Z., A.R. and C.H.O.; data curation, T.Z.; writing—original draft preparation, T.Z. and A.R.; writing—review and editing, T.Z. and A.R.; visualization, T.Z.; supervision, A.R. and C.H.O.; project administration, C.H.O.; funding acquisition, C.H.O.; All authors have read and agreed to the published version of the manuscript.

Funding: This research was funded by the Swiss Federal Office of Energy (Grant Nos. SI/501278-01 and SI/501300-01).

Data Availability Statement: The data presented in this study are available on request from the corresponding author.

Conflicts of Interest: The authors declare no conflict of interest.

Abbreviations

The following abbreviations are used in this manuscript:

CAN	Controller Area Network
CCHP	Combined Cooling, Heat and Power
CHP	Combined Heat and Power
ECU	Electronic Control Unit
HRSG	Heat Recovery Steam Generator
HXE	Heat exchanger exhaust gas
HXP	Plate heat exchanger
ICE	Internal Combustion Engine
mCHP	Micro Combined Heat and Power
MPC	Model Predictive Control
NLP	Nonlinear Program
OCP	Optimal Control Problem
ODE	Ordinary Differential Equation
PI	Proportional Integral
SISO	Single-Input Single-Output
TES	Thermal Energy Storage
TWC	Three-way Catalytic Converter

Symbols

The following symbols are used in this manuscript:

ϑ	temperature	[°C]
f	pump mass flow	[kg s^{-1}]
γ	valve split factor	[-]
m	mass	kg
$\dot{m}$	mass flow	[kg s^{-1}]
$\dot{Q}$	heat flow	[W]
c_p	isobaric specific heat capacity	[J kg^{-1} K^{-1}]
UA	lumped heat transfer coefficient and contact surface	[W K^{-1}]
kA	lumped heat transfer coefficient and contact surface	[W K^{-1}]
N	horizon	[-]

T_s	uniform time period between consecutive samples	[s]
k	discrete time index	[-]
η_{th}	thermal efficiency measure	[-]

Subscripts and Superscripts

The following symbols are used in this manuscript:

a	air
avg	average
byp	bypass
c	coolant
chp	combined heat and power plant
$cold$	cold
e	engine
exh	exhaust
hot	hot
hxe	heat exchanger exhaust
hxp	plate heat exchanger
in	entering
max	maximum
mid	middle
out	exiting
ref	reference
w	water

Appendix A

Table A1. Test rig hardware.

Component	Type	Range	Accuracy
Engine	1-cylinder, displacement volume 0.325 L, mechanical power $P_e = 7.7$ kW	-	-
Generator	EMWB AG, asynchronous, efficiency $\eta = 0.931$, $\cos(\phi) = 0.93$	-	-
HXP	Alfa Laval CBH16-25H plate heat exchanger	-	-
HXE	Prototype, gas-to-water heat exchanger, $V_{water} = 0.051\,\mathrm{m}^3$	-	-
Pumps	Wilo-Stratos PARA/-Z	-	-
3-way valves	Valves: Belimo R513, Electric Actuator: Belimo NRC24A-SR	-	-
ECU	Woodward ECM-0563-048-0701-C	-	-
Temperature Sensors	Thermocouple Type K	0 to 25 °C	±2.2 °C
Thermocouple Scanner	Axiomatic AXTC20	-	±1 °C
Flow Sensors	Vortex Flow Sensor 200	1.8 to 32 L/min	<2%
Gas Valve	Heinzmann E-LES 30 SMC	-	-
CAN Connector	Kvaser Leaf Light HS v2	-	-
Lab Computer	Dell Precision Tower 3620 XCTO, 20 GB RAM	-	-

Table A2. Model Parameters.

Parameter	Description	Value
$\dot{Q}_{comb,e}$	Heat flow to engine block due to combustion	1.16×10^5 W
$UA_{e,a}$	Lumped heat transfer coefficient and surface between engine block and ambient	1535.2 W K^{-1}
$UA_{e,c}$	Lumped heat transfer coefficient and surface between engine block and coolant	76.343 W K^{-1}
kA_{hxe}	Lumped heat transfer coefficient and heat exchange surface in exhaust gas heat exchanger	73.193 W K^{-1}
kA_{hxp}	Lumped heat transfer coefficient and heat exchange surface in plate heat exchanger	1275.4 W K^{-1}
$c_{p,c}$	Specific heat capacity of coolant fluid (water with 25% ethylene glycol)	1772.4 J kg^{-1} K^{-1}
$c_{p,e}$	Specific heat capacity of engine block	1807.9 J kg^{-1} K^{-1}
$c_{p,exh}$	Specific heat capacity of exhaust gas	10,044 J kg^{-1} K^{-1}
$c_{p,w}$	Specific heat capacity of water	1945.6 J kg^{-1} K^{-1}
$m_{c,e}$	mass of coolant fluid in engine	4.524 kg
$m_{c,hxp}$	mass of coolant fluid in plate heat exchanger	1.478 kg
m_e	mass of engine	25.696 kg
$m_{exh,hxe}$	mass of exhaust gas in heat exchanger	404.71 kg
$m_{w,supply}$	mass of water in supply pipe after plate heat exchanger	1.271 kg
$m_{w,hxe}$	mass of water in exhaust gas heat exchanger	115.21 kg
$m_{w,hxp}$	mass of water in plate heat exchanger	2.291 kg
$\dot{m}_{exh}$	exhaust gas mass flow	0.446 kg s^{-1}
$\vartheta^{in}_{exh,hxe}$	temperature of exhaust gas at inlet of exhaust gas heat exchanger	113.04 °C

References

1. IPCC. *Climate Change 2022: Mitigation of Climate Change. Contribution of Working Group III to the Sixth Assessment Report of the Intergovernmental Panel on Climate Change*; Cambridge University Press: Cambridge, UK; New York, NY, USA, 2022. [CrossRef]
2. Liu, M.; Shi, Y.; Fang, F. Combined cooling, heating and power systems: A survey. *Renew. Sustain. Energy Rev.* **2014**, *35*, 1–22. [CrossRef]
3. Maghanki, M.M.; Ghobadian, B.; Najafi, G.; Galogah, R.J. Micro combined heat and power (MCHP) technologies and applications. *Renew. Sustain. Energy Rev.* **2013**, *28*, 510–524. [CrossRef]
4. Murugan, S.; Horák, B. A review of micro combined heat and power systems for residential applications. *Renew. Sustain. Energy Rev.* **2016**, *64*, 144–162. [CrossRef]
5. Tan, D.; Meng, Y.; Tian, J.; Zhang, C.; Zhang, Z.; Yang, G.; Cui, S.; Hu, J.; Zhao, Z. Utilization of renewable and sustainable diesel/methanol/n-butanol (DMB) blends for reducing the engine emissions in a diesel engine with different pre-injection strategies. *Energy* **2023**, *269*, 126785. [CrossRef]
6. Zhang, Z.; Dong, R.; Lan, G.; Yuan, T.; Tan, D. Diesel particulate filter regeneration mechanism of modern automobile engines and methods of reducing PM emissions: A review. *Environ. Sci. Pollut. Res.* **2023**, *30*, 39338–39376. [CrossRef]
7. Angrisani, G.; Roselli, C.; Sasso, M. Distributed microtrigeneration systems. *Prog. Energy Combust. Sci.* **2012**, *38*, 502–521. [CrossRef]
8. Zhang, L.; Luo, Y. Combined heat and power scheduling: Utilizing building-level thermal inertia for short-term thermal energy storage in district heat system. *IEEJ Trans. Electr. Electron. Eng.* **2018**, *13*, 804–814. [CrossRef]
9. Rosato, A.; Sibilio, S.; Ciampi, G. Energy, environmental and economic dynamic performance assessment of different micro-cogeneration systems in a residential application. *Appl. Therm. Eng.* **2013**, *59*, 599–617. [CrossRef]
10. Pereira, J.S.; Ribeiro, J.B.; Mendes, R.; Vaz, G.C.; André, J.C. ORC based micro-cogeneration systems for residential application—A state of the art review and current challenges. *Renew. Sustain. Energy Rev.* **2018**, *92*, 728–743. [CrossRef]
11. Georg Bock, H.; Diehl, M.; Schlöder, J.P.; Allgöwer, F.; Findeisen, R.; Nagy, Z. Real-Time Optimization and Nonlinear Model Predictive Control of Processes Governed by Differential-Algebraic Equations. *IFAC Proc. Vol.* **2000**, *33*, 671–679. [CrossRef]
12. Mayne, D.Q. Model predictive control: Recent developments and future promise. *Automatica* **2014**, *50*, 2967–2986. [CrossRef]
13. Mohammadian, P.K.; Saidi, M.H. Simulation of startup operation of an industrial twin-shaft gas turbine based on geometry and control logic. *Energy* **2019**, *183*, 1295–1313. [CrossRef]
14. Sindareh-Esfahani, P.; Ghaffari, A.; Ahmadi, P. Thermodynamic modeling based optimization for thermal systems in heat recovery steam generator during cold start-up operation. *Appl. Therm. Eng.* **2014**, *69*, 286–296. [CrossRef]

15. Aurora, C.; Diehl, M.; Ferramosca, A.; Magni, L.; Miotti, A.; Scattolini, R. Nonlinear model predictive control for combined cycle power plants. *IFAC Proc. Vol.* **2004**, *37*, 621–626. [CrossRef]
16. Albanesi, C.; Bossi, M.; Magni, L.; Paderno, J.; Pretolani, F.; Kuehl, P.; Diehl, M. Optimization of the Start-up Procedure of a Combined Cycle Power Plant. In Proceedings of the 45th IEEE Conference on Decision and Control, San Diego, CA, USA, 13–15 December 2006. [CrossRef]
17. Tică, A.; Guéguen, H.; Dumur, D.; Faille, D.; Davelaar, F. Design of a combined cycle power plant model for optimization. *Appl. Energy* **2012**, *98*, 256–265. [CrossRef]
18. Casella, F.; Farina, M.; Righetti, F.; Faille, D.; Tica, A.; Gueguen, H.; Scattolini, R.; Davelaar, F.; Dumur, D. An optimization procedure of the start-up of Combined Cycle Power Plants. *IFAC Proc. Vol.* **2011**, *44*, 7043–7048. [CrossRef]
19. Larsson, P.O.; Casella, F.; Magnusson, F.; Andersson, J.; Diehl, M.; Akesson, J. A framework for nonlinear model-predictive control using object-oriented modeling with a case study in power plant start-up. In Proceedings of the 2013 IEEE Conference on Computer Aided Control System Design (CACSD), Hyderabad, India, 28–30 August 2013. [CrossRef]
20. Diaz, J.L.; Ocampo-Martinez, C.; Panten, N.; Weber, T.; Abele, E. Optimal operation of combined heat and power systems: An optimization-based control strategy. *Energy Convers. Manag.* **2019**, *199*, 111957. [CrossRef]
21. Wang, J.; You, S.; Zong, Y.; Træholt, C.; Dong, Z.Y.; Zhou, Y. Flexibility of combined heat and power plants: A review of technologies and operation strategies. *Appl. Energy* **2019**, *252*, 113445. [CrossRef]
22. Wang, W.; Liu, J.; Zeng, D.; Fang, F.; Niu, Y. Modeling and flexible load control of combined heat and power units. *Appl. Therm. Eng.* **2020**, *166*, 114624. [CrossRef]
23. Kazda, K.; Li, X. A Critical Review of the Modeling and Optimization of Combined Heat and Power Dispatch. *Processes* **2020**, *8*, 441. [CrossRef]
24. Salman, C.A.; Li, H.; Li, P.; Yan, J. Improve the flexibility provided by combined heat and power plants (CHPs) – a review of potential technologies. *e-Prime—Adv. Electr. Eng. Electron. Energy* **2021**, *1*, 100023. [CrossRef]
25. Gu, W.; Wu, Z.; Bo, R.; Liu, W.; Zhou, G.; Chen, W.; Wu, Z. Modeling, planning and optimal energy management of combined cooling, heating and power microgrid: A review. *Int. J. Electr. Power Energy Syst.* **2014**, *54*, 26–37. [CrossRef]
26. Zhang, G.; Cao, Y.; Cao, Y.; Li, D.; Wang, L. Optimal Energy Management for Microgrids with Combined Heat and Power (CHP) Generation, Energy Storages, and Renewable Energy Sources. *Energies* **2017**, *10*, 1288. [CrossRef]
27. Costa, A.; Fichera, A. A mixed-integer linear programming (MILP) model for the evaluation of CHP system in the context of hospital structures. *Appl. Therm. Eng.* **2014**, *71*, 921–929. [CrossRef]
28. dos Reis, E.P.; Arrieta, F.R.P.; Venturini, O.J. General methodology and optimization for the analysis of bottoming cycle cogeneration. *Energy Convers. Manag.* **2023**, *276*, 116536. [CrossRef]
29. Marrasso, E.; Roselli, C.; Sasso, M.; Tariello, F. Comparison of centralized and decentralized air-conditioning systems for a multi-storey/multi users building integrated with electric and diesel vehicles and considering the evolution of the national energy system. *Energy* **2019**, *177*, 319–333. [CrossRef]
30. Shakibi, H.; Shokri, A.; Assareh, E.; Yari, M.; Lee, M. Using machine learning approaches to model and optimize a combined solar/natural gas-based power and freshwater cogeneration system. *Appl. Energy* **2023**, *333*, 120607. [CrossRef]
31. Marseglia, G.; Medaglia, C.M.; Petrozzi, A.; Nicolini, A.; Cotana, F.; Sormani, F. Experimental Tests and Modeling on a Combined Heat and Power Biomass Plant. *Energies* **2019**, *12*, 2615. [CrossRef]
32. Yee, S.K.; Milanović, J.V.; Hughes, F.M. Validated Models for Gas Turbines Based on Thermodynamic Relationships. *IEEE Trans. Power Syst.* **2011**, *26*, 270–281. [CrossRef]
33. Laszczyk, P. Simplified modeling of liquid-liquid heat exchangers for use in control systems. *Appl. Therm. Eng.* **2017**, *119*, 140–155. [CrossRef]
34. Indumathy, M.; Sobana, S.; Panda, B.; Panda, R.C. Modelling and control of plate heat exchanger with continuous high-temperature short time milk pasteurization process—A review. *Chem. Eng. J. Adv.* **2022**, *11*, 100305. [CrossRef]
35. Gut, J.A.; Pinto, J.M. Modeling of plate heat exchangers with generalized configurations. *Int. J. Heat Mass Transf.* **2003**, *46*, 2571–2585. [CrossRef]
36. Damiani, L.; Revetria, R.; Giribone, P. A Dynamic Simulation Model for a Heat Exchanger Malfunction Monitoring. *Energies* **2022**, *15*, 1862. [CrossRef]
37. Mota, F.A.; Carvalho, E.; Ravagnani, M.A. Modeling and Design of Plate Heat Exchanger. In *Heat Transfer Studies and Applications*; InTech: Rijeka, Croatia, 2015. [CrossRef]
38. Andersson, J.A.E.; Gillis, J.; Horn, G.; Rawlings, J.B.; Diehl, M. CasADi – A software framework for nonlinear optimization and optimal control. *Math. Program. Comput.* **2019**, *11*, 1–36. [CrossRef]
39. Wächter, A.; Biegler, L.T. On the implementation of an interior-point filter line-search algorithm for large-scale nonlinear programming. *Math. Program.* **2006**, *106*, 25–57. [CrossRef]
40. Padua, D. (Ed.) MUMPS. In *Encyclopedia of Parallel Computing*; Springer: Boston, MA, USA, 2011; p. 1238. [CrossRef]
41. Bock, H.; Plitt, K. A Multiple Shooting Algorithm for Direct Solution of Optimal Control Problems. *IFAC Proc. Vol.* **1984**, *17*, 1603–1608. [CrossRef]
42. Kim, I.Y.; de Weck, O.L. Adaptive weighted sum method for multiobjective optimization: A new method for Pareto front generation. *Struct. Multidiscip. Optim.* **2006**, *31*, 105–116. [CrossRef]

43. Marler, R.T.; Arora, J.S. The weighted sum method for multi-objective optimization: New insights. *Struct. Multidiscip. Optim.* **2010**, *41*, 853–862. [CrossRef]
44. Scattolini, R. Architectures for distributed and hierarchical Model Predictive Control—A review. *J. Process Control* **2009**, *19*, 723–731. [CrossRef]